PERGAMON

Annals of Nuclear Energy 29 (2002) 235–253

annals of
NUCLEAR ENERGY

www.elsevier.com/locate/anucene

Instability localization with artificial neural networks (ANNs)

T. Tambouratzis *, M. Antonopoulos-Domis

Institute of Nuclear Technology, Radiation Protection, NCSR 'Demokritos', Aghia Paraskevi 153 10, Athens, Greece

Received 19 February 2001; received in revised form 14 March 2001; accepted 17 March 2001

Abstract

The aim of this piece of research is to investigate the potential of artificial neural networks (ANNs) for tackling the problem of instability localization. The instability is modeled by a variable strength absorber (point-source) in a two-dimensional bare reactor model with a one neutron-energy group. The proposed approach constitutes an exercise in simplicity in that: (1) an arbitrarily simplified model is employed for ANN training and validation; (2) few training and validation patterns of low complexity are utilized; (3) the ANN inputs are derived directly from the neutron noise signals, the proposed location of instability is given on-line via an uncomplicated combination of ANN outputs; (4) the ANN architecture is independent of the number of possible locations of instability. In fact, unlike previous approaches which employ hundreds of outputs (one for each fuel assembly), only two ANN outputs are employed representing the X- and Y-coordinates (location) of instability; (5) the responses of only a few detectors are employed; (6) a measure of confidence in the prediction is assigned. The results of ANN testing, which is performed on patterns from both actual and simplified models, are reported and analyzed.

1. Introduction

Local density wave oscillations in a BWR core give rise to neutron flux fluctuations in the nearby local power range monitors (LPRMs). Such oscillations induced by local channel thermal hydraulic instabilities (probably self-sustained coolant density wave oscillations) have been observed in practice, for instance at the Finnish

* Corresponding author. Tel.: +30-1-65-03-748; fax: +30-1-65-33-431.
E-mail address: tatiana@ipta.demokritos.gr (T. Tambouratzis).

0306-4549/02/$ - see front matter
PII: S0306-4549(01)00036-6

BWR TVO-1 in 1991 (D' Auria et al., 1997) and at the Swedish Forsmark-1 in 1997 (Engstrom, 1996; Karlsson and Pazsit, 1999). The aim of instability localization is to identify the position of the oscillations from the neutron noise signals; in fact, the ability to determine a rather small area within which the fuel assembly (or assemblies) with the instability lies is of obvious practical importance.

Research concerning the localization of neutron noise excitations has been reported for (a) a local absorber of variable strength and (b) the lateral vibration of an absorber rod. Three basic algorithms have been reported:

- Localization curves (Pazsit and Glockler, 1983, 1984, 1988). Their main disadvantage is that they are computationally intensive whereby on-line operation is not possible; additionally, due to the need for a subjective decision by an expert concerning the final localization, the algorithm cannot be fully automated.
- ANNs (Pazsit et al., 1996). The proposed approach is computationally intensive since the ANN is constructed with as many output nodes as there are possible points of instability.
- Function minimization (Karlsson and Pazsit, 1999). The location of instability is determined as the location for which the absolute difference between the spectral values of detector measured response and model estimation response is minimal for each reactor radial position.

The aim of this piece of research is to investigate the potential of artificial neural networks (ANNs) — and especially the back-propagation (BP) architecture — for tackling the problem of instability localization. The instability is modeled by a variable strength absorber point-source. The proposed approach constitutes an exercise in simplicity in that:

- A two-dimensional bare reactor model with a one neutron-energy group is employed as the "actual physical system".
- A model of the "actual physical system" is employed for training and validation of the ANNs employed for instability localization.
- The responses of only a few (four) detectors are employed.
- The ANN inputs are derived directly from the neutron noise signals (uncomplicated pre-processing), the proposed location of instability is given on-line via a direct combination of ANN outputs.
- The ANN architecture is independent of the number of possible locations of instability. In fact, unlike previous approaches which employ hundreds of outputs (one for each fuel assembly), only two ANN outputs are employed representing the X- and Y-coordinates (location) of instability.
- Few patterns of low complexity are utilized for ANN training and validation.
- A measure of confidence (i.e. a measure of expected error) in the prediction is assigned; this measure is related to the distance of the proposed location of instability from the centre of the reactor.

This paper is structured as follows. Section 2 briefly presents ANNs and the BP architecture. Section 3 describes the employed method as well as the two models

(namely the "actual physical system" and its simplification) from which the patterns utilized for ANN training, validation and testing are derived. The BP ANNs constructed for instability localization are presented in Section 4: training (employing patterns from the simplified model only) is described initially, followed by testing (employing patterns from both models). Section 5 concludes the paper.

2. Artificial neural networks (ANNs)

ANNs (Haykin, 1994) constitute a collection of parallel (i.e. fast, on-line) algorithms that are inspired by the structure of the human (or animal) brain and strive to simulate its operation on tasks where traditional information-processing techniques are either not successful or sub-optimal.

ANNs are composed of non-linear nodes which are richly interconnected and communicate with each other via weighted connections. The weights of the connections are used to store the knowledge concerning the task to be solved. During ANN training (only supervised training is considered here), knowledge is presented to the ANN in the form of patterns for which both their inputs (environmental knowledge) and outputs (desired response) are known. Knowledge acquisition is accomplished by modifying the weights of the connections in such a manner that the desired response of each training pattern is output when the corresponding input is presented to the ANN (in practice the aim is to adjust the weights so that the ANN output is moved sufficiently close to the desired response for all patterns). By the appropriate selection of the training patterns and by the correct application of a training procedure, the input-output mapping of the task is captured by the ANN, which is subsequently capable of responding accurately when presented with novel inputs. Owing to the distributed nature of knowledge-storage, the ANN is endowed with fault tolerance and robustness to noise: the ANN is capable of responding in a satisfactory manner even when the inputs are partly missing or distorted or when some of the weights have degraded.

A BP ANN (Rumelhart et al., 1986) is implemented here for tackling the problem of instability localisation.

3. The method

The proposed method follows the principles of any ANN application (or indeed, any methodology where modification/adjustment of the model-determining parameters is involved): data in the form of appropriately transformed input–output pairs are used for training, validation and — subsequently — testing. For the instability localization problem, logarithms of ratios of detector responses — to be called from now on response-ratios — constitute the ANN inputs, while the X- and Y-coordinates (location) of instability constitute the ANN outputs.

A problem that frequently occurs in practice is that there are not sufficient — if any — measurements of the variables of interest of the physical system which can be

transformed and subsequently used as ANN training and validation patterns. It is, thus, necessary to resort to model(s) of the physical system. Two points are in order here concerning model selection:

(a) The effectiveness/robustness of the method is sensitive to the degree of closeness between the model and the actual physical system; this holds for any method.
(b) In many cases, data produced by the model are also considered as the experimental data for testing the method; hence the method incorporates exactly the same model in its solving algorithm. This testing procedure ignores that any model differs from the physical system, a fact that is further obscured since training and testing with the same model — barring erroneous training — cannot be anything less than "perfect".

In fact, not one but two models have been used here:

- A model (Section 3.1.1.) considered as the physical system and employed for deriving the "experimental data", i.e. the test patterns.
- A model (Section 3.1.2.) representing a simplification (rough approximation) of the physical system and employed for deriving the training and validation patterns.

3.1. The models

3.1.1. The "actual physical system"

A bare homogeneous critical two-dimensional reactor model with a one neutron-energy group is considered to be the "actual physical system" and its results to be the actual experimental data. The neutron flux fluctuations $\delta\Phi(\underline{r}, t)$, following linearization, are determined by the equations

$$\frac{\mathrm{d}\delta\Phi(\underline{r}, t)}{\mathrm{d}t} = \upsilon.D.\nabla^2\delta\Phi(\underline{r}, t) + b^2.\delta\Phi(\underline{r}, t) - \upsilon.\Phi_o(\underline{r}).\delta\Sigma_a(\underline{r}, t) + \lambda.\upsilon.\delta C(\underline{r}, t) \tag{1a}$$

$$\frac{\mathrm{d}\delta C(\underline{r}, t)}{\mathrm{d}t} = \beta.k_\infty.\Sigma_{a_o}(\underline{r}).\delta\Phi(\underline{r}, t) - \lambda.\delta C(\underline{r}, t) \tag{1b}$$

$$b^2 = [(1-\beta).k_\infty - 1].\Sigma_{a_o}(\underline{r}).\upsilon \tag{1c}$$

where the symbols have their usual meaning, $\delta C(\underline{r}, t)$are the delayed neutron percursor density fluctuations and $\delta\Sigma_a(\underline{r}, t)$ are the absorption cross-section fluctuations exciting the system; $\Phi_o(\underline{r})$ is the static neutron flux. The solution of the system is obtained as a sum of space-time harmonics, namely,

$$\begin{aligned}\delta\Phi(\underline{r}, t) &= \sum_{n=1,m=1}^{\infty} X_n(x).Y_m(y).T_{n,m}(t)\\ \delta C(\underline{r}, t) &= \sum_{n=1,m=1}^{\infty} X_n(x).Y_m(y).Q_{n,m}(t)\end{aligned} \tag{2}$$

where X_n, Y_m are the orthonormal eigenfunctions of the system satisfying the relevant Helmholtz equation and the boundary conditions of zero flux at the extrapolated boundaries of the reactor core. Fourier transforming (1) and (2), substituting (2) into (1) and using the orthonormality properties of $X_n(x)$ and $Y_m(y)$, the Fourier transform $\delta\overline{\Phi}(\underline{r}, \omega)$ of $\delta\Phi(\underline{r}, t)$ reads

$$\delta\overline{\Phi}(x, y, \omega) = \sum_{n=1,m=1}^{600} X_n(x).Y_m(y).\overline{T_{n,m}}(\omega) \tag{3}$$

where $n = m = 600$ the number of harmonics for which the particular system converges well.

A critical rectangular reactor of dimensions 289×289 cm^2 has been considered. Bearing in mind that flow instabilities at BWRs appear at about 0.4–0.5 Hz, (3) has been evaluated at $\omega = \pi$.

3.1.2. The simplified model

The neutronic response $NR(\underline{r_D}, \underline{r_s})$ at position $\underline{r_D}$ (detector point) to a point variable strength absorber at position $\underline{r_s}$ (excitation point) has been modeled by

$$NR(\underline{r_D}, \underline{r_s}) = S_o.\mathrm{e}^{-\frac{\left|\underline{r_D} - \underline{r_s}\right|}{L}} \tag{4}$$

where S_o is the source strength and L is a relaxation length to be estimated. Response-ratios of the simplified model take the form

$$\ln\left(\frac{NR\left(\underline{r_{D_1}}, \underline{r_s}\right)}{NR\left(\underline{r_{D_2}}, \underline{r_s}\right)}\right) = \frac{\left|\underline{r_{D_2}} - \underline{r_s}\right| - \left|\underline{r_{D_1}} - \underline{r_s}\right|}{L} \tag{5}$$

whereby the source strength S_o is eliminated, while L acts directly as a scaling factor.

A prerequisite for the evaluation of the response-ratios of the simplified model is the estimation of L. The value of L must be near the value of the relaxation length L_g of the global component. This has been estimated in the plateau frequency region for this reactor configuration as $L_g = 30.547$ cm (Behringer et al., 1997). The actual value of L_g is expected to depend on the size of the reactor and on the frequency ω and can be experimentally measured and/or computed using models of the reactor. Assuming that the "actual physical system" is determined by (1), L_g can be deduced from Green's function $G(\underline{r}, \underline{r_s}, \omega)$ of (1), where $\underline{r}$ is a point in the reactor. L must be such that the right-hand side of (4) approximates G, i.e.

$$G_N(\underline{r}, \underline{r_s}, \omega) = \mathrm{e}^{-\frac{\left|\underline{r} - \underline{r_s}\right|}{L(\omega)}} \tag{6}$$

where $G_N(\underline{r}, \underline{r_s}, \omega)$ is the magnitude (absolute value) of Green's function $G(\underline{r}, \underline{r_s}, \omega)$ normalized to $G(\underline{r_s}, \underline{r_s}, \omega)$. Taking the logarithm of (6) reads

$$\ln\left(G_N\left(\underline{r}, \underline{r_s}, \omega\right)\right) = -\frac{\left|\underline{r} - \underline{r_s}\right|}{L(\omega)} \tag{7}$$

or

$$1/L(\omega) = \frac{-\ln G_N\left(\underline{r}, \underline{r_s}, \omega\right)}{\left|\underline{r} - \underline{r_s}\right|} \tag{8}$$

i.e. $1/L$ must approximate the slope of $\ln(G_N)$.

G_N has been evaluated at $\omega = \pi$ for a variety of $\underline{r_s}$ positions, ranging from the centre to the boundaries of the reactor. It is illustrated here [Figs. 1(b) and 2(b)] for two $\underline{r_s}$ positions — one located at the centre of the reactor $\underline{r_s} = (144.5, 144.5)$, the other located near the boundaries of the reactor $\underline{r_s} = (25, 25)$ — and for $\underline{r}$ positions along the lines shown in Figs. 1(a) and 2(a), respectively. For ease of viewing, $\ln(G_N)$ and the corresponding L are illustrated separately on either side of the peak [Figs. 1(c) and 2(c) for the left-hand side and Figs. 1(d) and 2(d) for the right-hand side, respectively].

As expected — and as can be seen in Fig. 1(c) and (d) — , G_N varies exponentially with $\left|\underline{r} - \underline{r_s}\right|$ a few diffusion lengths away from the point $\underline{r_s}$ of excitation. As also expected near (a few diffusion lengths) the boundaries of the reactor, $G_N\left(\underline{r}, \underline{r_s}, \omega\right)$ reduces much more rapidly than the exponential function, a fact that is due to the boundary conditions. Because the excitation position $\underline{r_s}$ is at the centre of the reactor

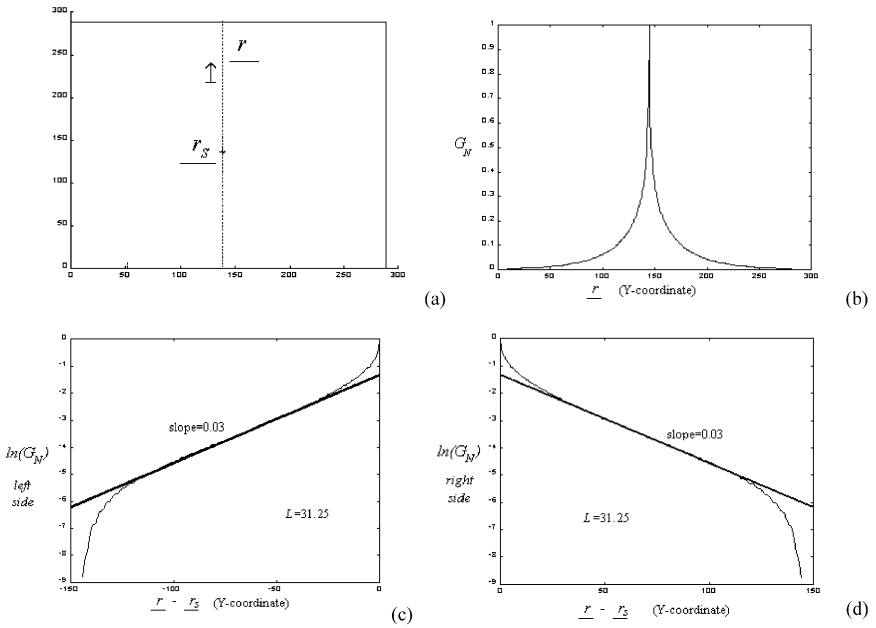

Fig. 1. Green's function evaluation and L calculation for $\underline{r_s}$ at the centre of the reactor.

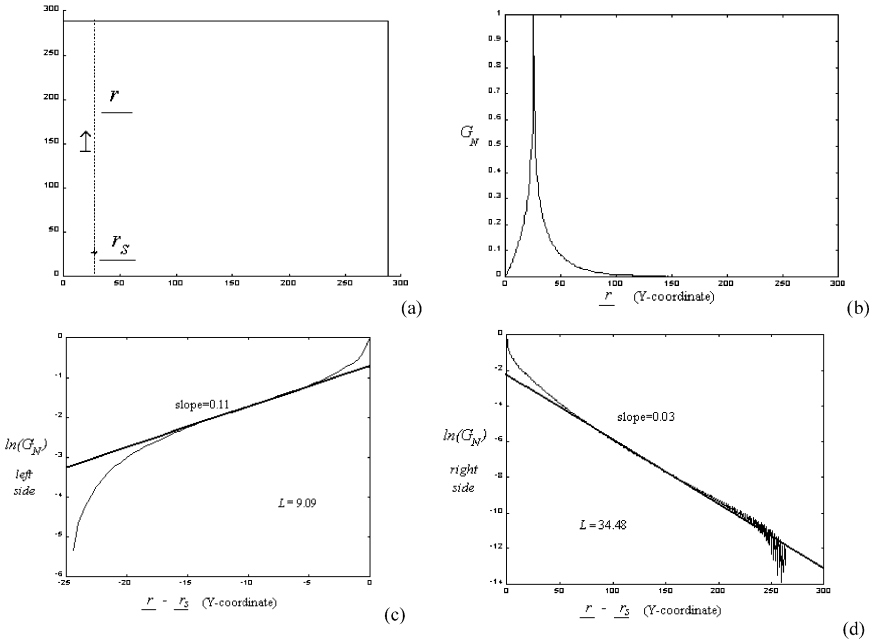

Fig. 2. Green's function evaluation and L calculation for $\underline{r_s}$ near the boundaries of the reactor.

[Fig. 1(a)], G is symmetric with respect to $\underline{r_s}$. From the slope of $\ln(G_N)$ away from $\underline{r_s}$ as well as the boundaries, the relaxation length is estimated as $L = 31.25$ cm, i.e. near L_g.

It has generally been observed that for excitation points away (many diffusion lengths) from the boundaries, the relaxation lengths L — evaluated away from the boundaries and the excitation point $\underline{r_s}$ — lie in the range 30–35 cm, i.e. are near L_g. For excitation points near the boundaries of the reactor (e.g. Fig. 2):

- The part of the curve from the excitation to the boundaries is significantly affected by the boundary conditions and, consequently, any relaxation length derived from that part is much smaller than L_g [Fig. 2(c)].
- The relaxation length derived from the other part of the curve [Fig. 2(d)] lies in the range 30–35 cm, i.e. is near L_g. The observed oscillations at the right part of Fig. 2(d) are due to numerical errors caused by the corresponding G_N values approaching 0.

Hence, the range 30–35 cm for L enables the simplified model to approximate Green's function of the "actual physical system", except in cases where either $\underline{r}$ or $\underline{r_s}$ lie near the boundaries of the reactor, or $\underline{r}$ and $\underline{r_s}$ lie near each other.

Subsequently, fitting of (4) with L from within the aforementioned range to curves derived from the "actual physical system" is not expected to always be satisfactory. Neutronic response curves from the "actual physical system" have been collected for

a variety of detector positions $\underline{r_D}$; for each selected $\underline{r_D}$, the variable strength absorber positions $\underline{r_s}$ have been moved along lines of different orientations where — additionally — $\min(|\underline{r_D} - \underline{r_s}|)$ has been varied from 0 to small, moderate and large values. Fitting of (4) has been attempted for each normalized curve of the "actual physical system" [whereby $S_o = 1$ in (4)] and separately on each side of the peak. The quality of fit has been found dependent on both $\underline{r_D}$ and $\underline{r_s}$. Fitting is not at all possible when either detector and/or instability lie near the boundaries of the reactor. When $\min(|\underline{r_D} - \underline{r_s}|) = 0$ or very small, fitting is improved by moving about two diffusion lengths away from the peak and fitting from then onward [thus removing the peaking effect of Figs. 1(c) and (d) and 2(c) and (d)]. Fig. 3 illustrates fitting of (4) using $L = 33$ cm to the normalized neutronic response curve of Fig. 3(b) derived from a fixed $\underline{r_D} = (51, 51)$ and from $\underline{r_s}$ moving along the line shown in Fig. 3(a). Fitting along the left part of the curve is not possible (owing to $\underline{r_s}$ being near the boundaries of the reactor), while fitting along the right part is shown in Fig. 3(c) and — subsequently — in Fig. 3(d) when moving two diffusion lengths away from the peak.

Finally, a "best fit" of (5) to the response-ratios of the "actual physical system" has been performed. A variety of pairs of detector positions $\underline{r_D}$ and variable strength absorber positions $\underline{r_s}$ have been tested, employing L values from within the range 30–35 cm. A significant deviation between the response-ratios of the two models occurs — for all tested L values — when

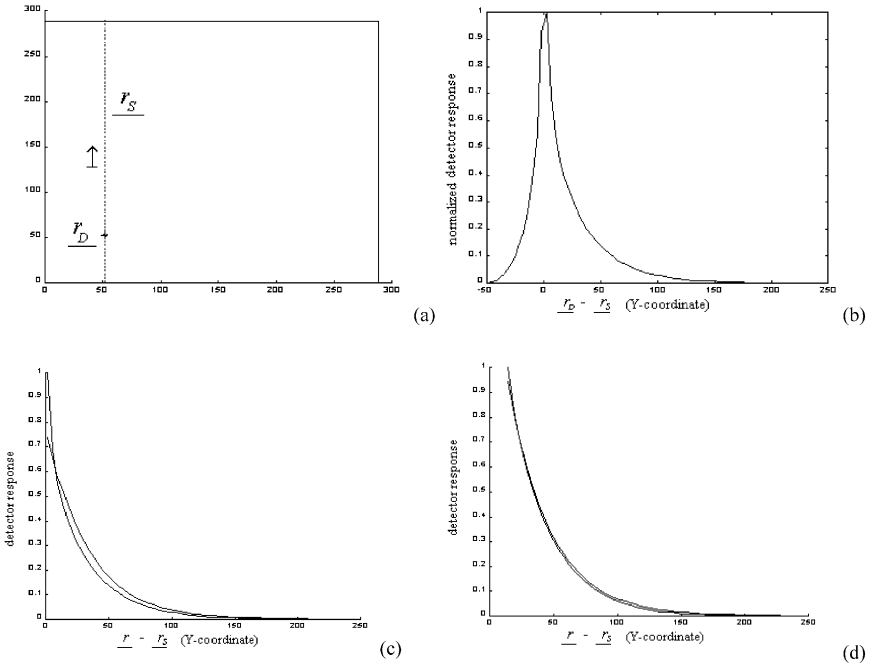

Fig. 3. Normalized neutronic response curve (b) derived from $\underline{r_D}$ and the $\underline{r_s}$ positions shown in (a); fitting of (4) with $L = 33$ to the right part of the curve (c) and (d).

- $|\underline{r_D} - \underline{r_s}|$ is zero or very small, i.e. the location of instability lies in the vicinity of either of the detectors [as for the response-ratios of Fig. 4(b) that correspond to $\underline{r_s}$ positions in the vicinity of $\underline{r_{D_1}} = (239, 239)$ in Fig. 4(a)], or
- the instability lies near the boundaries of the reactor [as for the response-ratios of Fig. 4(d) that correspond to $\underline{r_s}$ positions near the boundaries in Fig. 4(c)].

In the following, $L = 33$ cm has been used for the calculation of the response-ratios of the simplified model.[1]

3.2. Detector selection

3.2.1. Number

For either model, a single detector — even for a known S_o in (4) — can only perform localization on a closed curve (for the simplified model the closed curve constitutes a circle of a given radius); two detectors perform ambiguous localization

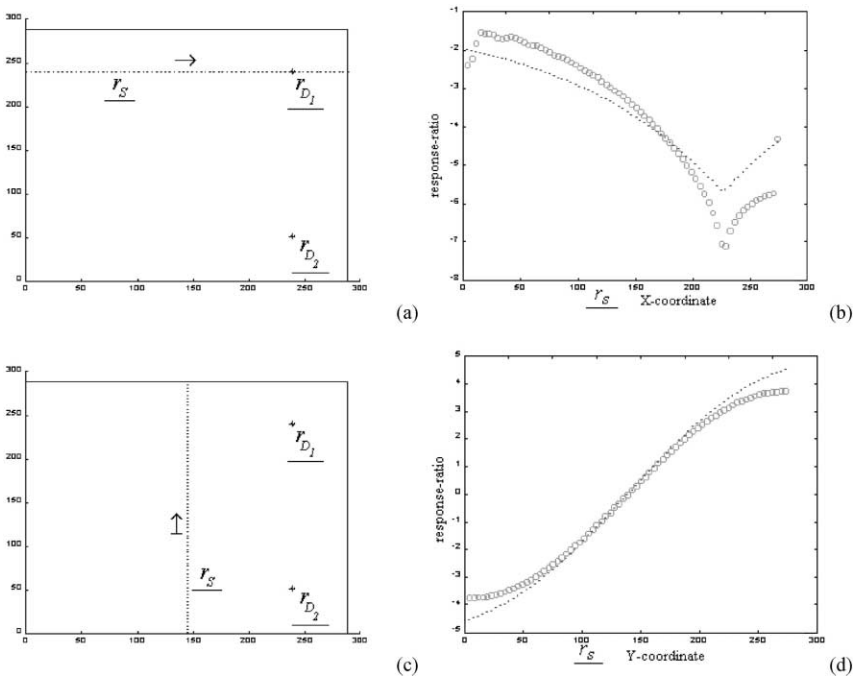

Fig. 4. Examples of the deviations between response-ratios of the two models; the circles correspond to the response-ratios of the "actual physical system", while the dots correspond to the response-ratios (5) of the simplified model for $L = 33$.

[1] Fig. 4(d) gives an example of the nature of match between the two response-ratio curves for $L = 33$ cm. Owing to the fact that L acts as a scaling factor from (5), the choice of a larger L would cause significant deviations between the two response-ratio curves in the centre of the reactor, while the choice of a smaller L would further accentuate the discrepancy near the boundaries of the reactor.

(for the simplified model two $\underline{r_S}$ positions are proposed lying in symmetrical positions relative to the line connecting the detectors); three detectors is the minimum requirement for unambiguously performing instability localization. Four detectors have been employed here, as they have been found to allow for significantly more accurate instability localization than three (a finding also mentioned in Karlsson and Pazsit, 1999).

It has been decided not to use more detectors since the resulting detector configurations produce more reactor areas associated with discrepancies in the response-ratios of the two models (one area in the vicinity of each detector position).

3.2.2. Location

As shown in Fig. 5, the four detectors have been placed at positions symmetrical to the centre of the reactor $\underline{r_{D_1}} = (51, 51)$, $\underline{r_{D_2}} = (239, 51)$, $\underline{r_{D_3}} = (51, 239)$ and $\underline{r_{D_4}} = (239, 239)$. Their positions have been selected 50 cm away from the boundaries of the reactor (following the findings of Section 3.1.2), while they are spaced out and not near each other. This detector configuration has been found to produce the most appropriate ANN inputs (response-ratios) for the proposed approach.

4. BP ANNs for instability localization

The ANN patterns, which comprise response-ratios as their inputs and the X- and Y-coordinates of the location of instability as their outputs, have been employed for:

- Training and validation. Only the simplified model has been used for the production of the training and validation patterns. The training patterns have been selected as 1 out of every 100 consecutive points on the raster-scanned grid of the reactor, where neigbouring points are separated by 1cm along both the X- and Y-axes; the validation patterns constitute the middle points — again on the raster-scanned grid — of the training patterns. This sparse sampling results in 836 training and 835 validation patterns (some extended training sets are presented in Section 4.2).

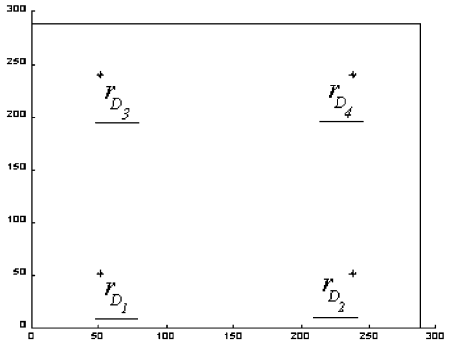

Fig. 5. Detector configuration.

- Testing. Both models have been used for the production of the test patterns. The test patterns of the simplified model have been employed to verify that a correct ANN architecture and an adequate (fully representative of the problem) training set have been selected as well as that the input-output mapping of the task has been successfully captured by the trained BP ANNs. The test patterns of the "actual physical system" determine the effect that the deviation between the two models has on ANN operation, i.e. how well the simplified model actually captures the characteristics of the "actual physical system" for the purposes of instability localization. A total of 1460 test patterns from each model have been used; their actual positions $\underline{r_S}$ are shown in Fig. 6.

4.1. BP ANN training

The pairwise combination of the four detectors $\underline{r_{D_1}}$, $\underline{r_{D_2}}$, $\underline{r_{D_3}}$ and $\underline{r_{D_4}}$ of Fig. 5 produces six response-ratios D_4/D_1, D_4/D_2, D_4/D_3, D_3/D_1, D_3/D_2 and D_2/D_1. Different configurations of response-ratios have been tried as BP ANN inputs, ranging from information-loaded configurations (e.g. employing all six response-ratios simultaneously) to information-specific configurations (e.g. employing a single response-ratio only). Of them, the configuration of two response-ratios (necessarily covering three out of the four detectors) has been selected as input to the BP ANN.

For every combination of three detectors (for instance detectors $\underline{r_{D_2}}$, $\underline{r_{D_3}}$ and $\underline{r_{D_4}}$ in Fig. 7, whereby $\underline{r_{D_1}}$ is excluded), three response-ratios are available ($\overline{D_4/D_2}$, $\overline{D_4/D_3}$ and D_3/D_2 in Fig. 7) resulting in three pairs of response-ratios (D_4/D_2 and D_4/D_3, D_4/D_3 and D_3/D_2, D_4/D_2 and D_3/D_2, marked in Fig. 7 by bold lines, lines with circles and dotted lines, respectively). The choice of pair of response-ratios for a given combination of three detectors has been found to have no effect either on BP ANN training (identical ANN architecture, comparable e_{av} values) or on testing. This implies that the relative distance of the selected pairs of detectors does not significantly affect BP ANN performance — at least for the employed reactor and detector configuration. For uniformity, the response-ratios with equal distances between each

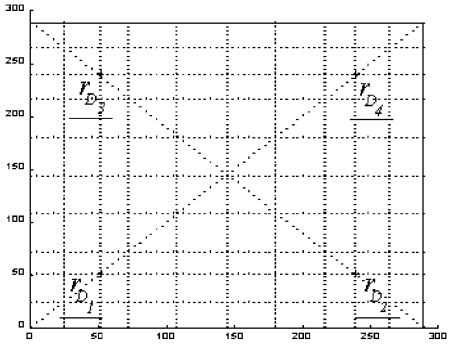

Fig. 6. 1460 Test patterns, arranged into 20 lines (9 horizontal, 9 vertical and 2 diagonal) of 73 patterns each.

pair of detectors have been selected as inputs to the BP ANN (D_4/D_2 and D_4/D_3 in Fig. 7).

Four BP ANNs have been trained for the instability localization problem, one for each combination of three detectors (i.e. one for each excluded detector). Each ANN is of structure 2–13–2, i.e. comprises two inputs (the two response-ratios), a single hidden layer with 13 nodes and two outputs (X- and Y-coordinates of the predicted location of instability). The sigmoid activation function, the batch mode of training, $\alpha = 0.9$, $\eta = 0.1$, scaling of the inputs in the interval $(-2.5, 2.5)$ and of the outputs in the interval [0.1, 0.9], and weight initialization in the interval $[-0.05, 0.05]$ have been performed. Training is terminated when either of the following is fulfilled:

- The average error (e_{av}) of the training and/or validation set begins to increase.
- Both average errors reach a small value and cease to significantly decrease.
- The number of training epochs exceeds 10,000.

The number of training epochs and the e_{av} values of the training and validation sets are shown in Table 1 for the four trained BP ANNs.

4.2. BP ANN testing

4.2.1. Simplified model

Each of the four trained BP ANNs constitutes an accurate predictor of the location of instability for the test patterns of the simplified model. The mean and maximum

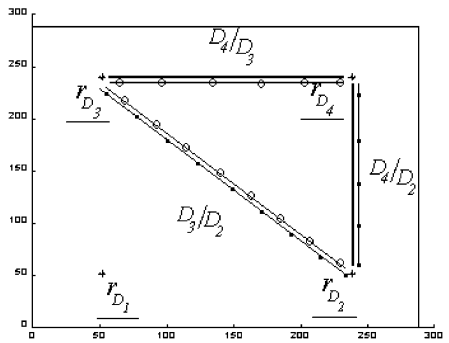

Fig. 7. Response-ratios for detectors $\underline{r_{D_2}}$, $\underline{r_{D_3}}$ and $\underline{r_{D_4}}$.

Table 1
BP ANN training characteristics

BP ANN	Inputs	Epochs	e_{av} (training)	e_{av} (validation)
1	D_4/D_2 and D_4/D_3	9000	0.000201	0.000524
2	D_3/D_1 and D_4/D_3	10000	0.000215	0.000620
3	D_2/D_1 and D_4/D_2	10000	0.000214	0.000596
4	D_2/D_1 and D_3/D_1	10000	0.000232	0.000482

distance between actual and predicted location of instability for BP ANN 1 (with $\underline{r_{D_1}}$ excluded from the response-ratios) are shown in the first row of Table 2, while a histogram of the distances is illustrated in Fig. 8 (dark bars).

An example of instability localization is given in Fig. 9(a) for BP ANN 1 and three distinct — but characteristic — $\underline{r_S}$ positions, one near the centre of the reactor and two near the boundaries of the reactor (one near the excluded detector and the other near one of the detectors considered in the response-ratios of the BP ANN inputs); the actual locations of instability are marked by circles, while the corresponding BP ANN 1 predictions are marked by crosses.

Fig. 10(a) further illustrates the actual (circles) and BP ANN 1 predicted (dots) locations of instability for the 1460 patterns of the test set. It can be seen that prediction accuracy is higher in the central area of the reactor as well as in the part (quadrant) of the reactor closest to the excluded detector. The observed fall in accuracy near the remaining three corners of the reactor is explained by the following: for those locations of instability, either one or both response-ratios lie at the ends of the BP ANN input range; the predictive power of the BP ANN is not always high at these limits since the number of training patterns in the vicinity is limited.[2] Conversely, the response-ratios in the quadrant of the excluded detector are numbers well within the input range (where a considerable number of training patterns exist), whereby prediction accuracy is high.

The quadrant-dominance combination of the four BP ANN predictions has subsequently been employed for instability localization: depending on the quadrant of the reactor into which the location of instability falls according to the average of the four BP ANN predictions, the location of instability is given by the BP ANN for which the detector lying in this quadrant is excluded from the response-ratios. Quadrant-dominance produces superior results, as shown in the histogram of Fig. 8 (light bars), in Figs. 9(b) and 10(b) and in the third row of Table 2; in fact, quadrant-dominance

Table 2
Distance characteristics between actual and predicted locations of instability for the 1460 test patterns of the simplified model

BP ANN	Mean distance (cm)	Maximum distance (cm)
1	5.51	52.04
1 On extended training set	1.97	12.56
Quadrant-dominance	2.56	11.92

[2] The decline in prediction accuracy for patterns at the ends of the input ranges constitutes a usual problem with ANNs. A solution is to employ extended training sets involving more patterns from the ends of the input ranges. Such an extended set was created here with the training patterns selected as 1 out of every 30 (instead of 100) consecutive points on the raster-scanned grid of the reactor for the area of the reactor outside the detectors (1130 patterns), and 1 out of every 100 consecutive points on the raster-scanned grid for the area of the reactor between the detectors (same 357 patterns as in the original training set), totalling 1487 training patterns; the validation set was not altered. Superior results were produced (see second row of Table 2), but more complex BP ANNs were required (2–18–2) with longer training times.

obliterates the need to employ extended training sets (footnote 2) and, subsequently, more complex ANNs. It is concluded that the four BP ANNs have been correctly constructed and trained for the instability localization problem and can be employed

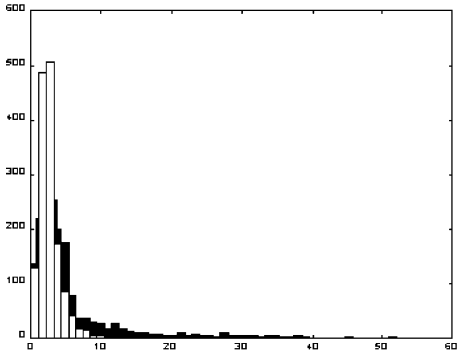

Fig. 8. Histograms of the distances between actual and predicted locations of instability for BP ANN 1 (dark bars) and quadrant-dominance (light bars).

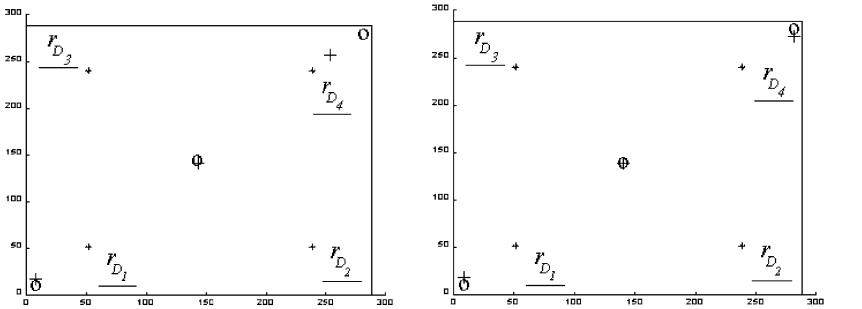

Fig. 9. Predictions (crosses) of representative locations of instability (circles) by BP ANN 1 (a) and quadrant-dominance (b).

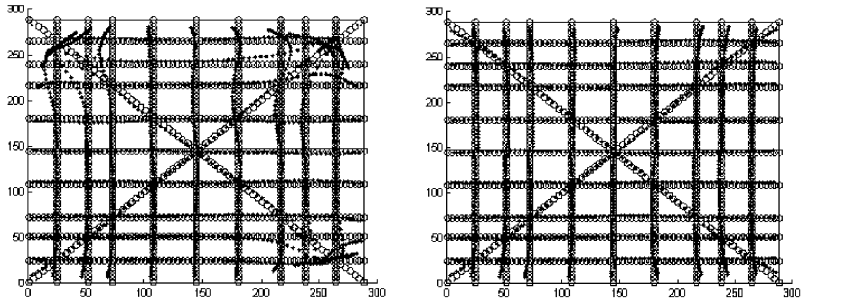

Fig. 10. Predictions (dots) of the 1460 actual locations of instability (circles) of the test set by BP ANN 1 (a) and quadrant-dominance (b).

for accurate instability localization of $\underline{r_s}$ positions from response-ratios derived from the simplified model. It is mentioned that comparable results have been arrived at when training, validating and testing with patterns from the "actual physical system".

4.2.2. "Actual physical system"

Unlike the results of Section 4.2.1, the four BP ANNs do not constitute accurate predictors of the location of instability for the test patterns of the "actual physical system".

An example of instability localization is given in Fig. 11(a) for BP ANN 1 and four locations of instability, one near the centre of the reactor, two near the boundaries of the reactor (one near the excluded detector and the other near one of the detectors considered in the response-ratios of the BP ANN inputs) and the last one in the vicinity of a detector considered in the response-ratios. The first three actual locations of instability are marked by circles, with the corresponding BP ANN 1 predictions marked by crosses, while the last actual location of instability is marked by a filled circle and the corresponding prediction by an ×.

Fig. 12(a) further illustrates the actual (circles) and BP ANN 1 predicted (dots) locations of instability for the 1460 patterns of the test set. It can be seen that instability localization is satisfactory only at the very centre of the reactor and degrades as the instability moves away from the centre and approaches the boundaries of the reactor. Severe shrinkage of the prediction towards the centre occurs in the part (quadrant) of the excluded detector as well as near the boundaries of the reactor. Conversely, an extension towards — and even outside — the boundaries of the reactor is observed for locations of instability in the vicinity of either of the detectors considered in the response-ratios.

The mean and maximum distance between actual and predicted location of instability are shown in the first row of Table 3, while a histogram of the distances is illustrated in Fig. 13 (dark bars). The utilization of extended training sets (footnote 2) produced no improvement on prediction accuracy. Furthermore, the quadrant-dominance combination of the four BP ANN predictions has been found unsuccessful in instability localization. This is due to the fact that, as shown in Fig. 12(a)

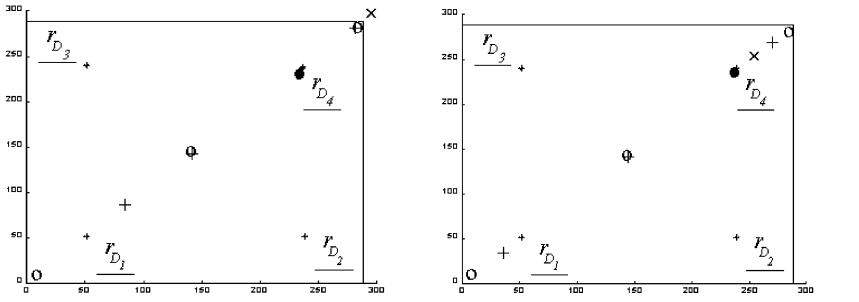

Fig. 11. Predictions (crosses and ×) of representative locations of instability (circles) by BP ANN 1 (a) and averaging (b).

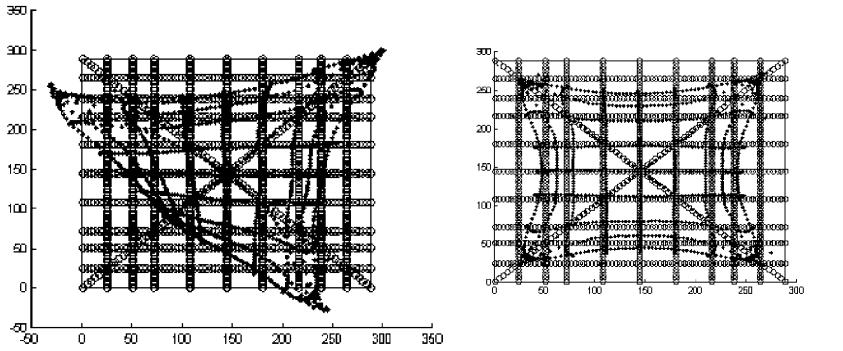

Fig. 12. Predictions (dots) of the 1460 locations of instability (circles) of the test set by BP ANN 1 (a) and averaging (b).

Table 3
Distance characteristics between actual and predicted locations of instability for the 1460 test patterns of the "actual physical system"

BP ANN	Mean distance (cm)			Maximum distance (cm)		
1	27.48			121.51		
		Partition			Partition	
Averaging	12.52	Central	2.86	80.71	Central	6.50
		Intermediate	8.68		Intermediate	43.63
		Near-boundary	18.50		Near-boundary	80.71

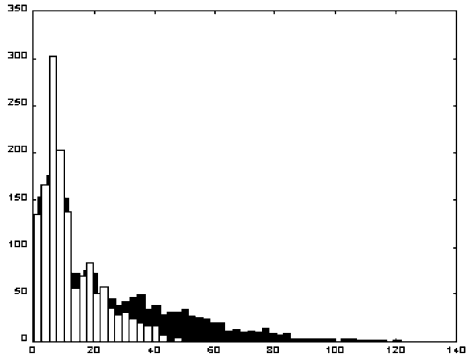

Fig. 13. Histograms of the distances between actual and predicted locations of instability for BP ANN 1 (dark bars) and averaging (light bars).

for BP ANN 1 and $\underline{r_{D_1}}$, the prediction of each BP ANN is mostly impaired in the quadrant corresponding to the excluded detector. It is thus clear that the impairment in instability localization when testing on data from the "actual physical system" is a

matter of characteristic differences (i.e. discrepancy between response-ratios) of the two models.

A simple averaging of the four BP ANN predictions significantly improves the accuracy of instability localization. This is shown in Figs. 11(b) and 12(b): prediction of the location of instability is satisfactory in the central area of the reactor, while it is still shrunk — but to a lesser degree — near the boundaries of the reactor; finally, prediction is still extended — again to a lesser degree — when the instability is located in the vicinity of either detector. The mean and maximum distance between actual and predicted (via BP ANN averaging) location of instability are shown in the second row of Table 3 while a histogram of the distances is illustrated in Fig. 13 (light bars).

For averaging, both mean and maximum distances are related to the predicted location of the instability within the reactor. The highlighted rows of Table 3 tabulate the mean and maximum distances in three distinct partitions of the reactor: a central partition (between points (100, 190), (190, 100), (100, 190) and (190, 190)), an intermediate partition, and a near-boundary partition [outside points (50, 50), (240, 50), (50, 240) and (240, 240)]. The further the predicted location of instability from the center of the reactor, the greater its mean and maximum distance from the actual location of instability, i.e. the larger the prediction error expected. Hence, a measure of confidence (i.e. a measure of expected error) in the prediction can be assigned, depending on the partition within which the prediction lies.

It can be concluded that the discrepancy between the "actual physical system" and the simplified model constitutes the sole reason for the problems in instability localization encountered at the outer areas of the reactor. Despite this, (a) accurate localization is performed when the instability is located in the central area of the reactor, (b) approximate localization is possible in the remaining parts of the reactor, in which case a measure of confidence (expected error) in the prediction is assigned.

5. Conclusions

Instability localization has been investigated using ANNs. A single instability has been considered at any instant and two models have been employed: a model representing the "actual physical system" and a simplified model assumed to capture the essential aspects of the "actual physical system". The patterns employed during ANN training and validation have been derived exclusively from the simplified model, while patterns from both models have been used for testing.

The proposed approach constitutes an exercise in simplicity in that:

(a) The responses of only four detectors are employed.
(b) Few patterns of low complexity are utilized for training and validation.
(c) The ANN inputs are derived directly from the neutron noise signals, the proposed location of instability is given on-line via a direct combination of ANN outputs.
(d) The ANN architecture is independent of the number of possible locations of

instability. In fact, unlike previous approaches which employ hundreds of outputs (one for each fuel assembly), only two ANN outputs are employed representing the X- and Y-coordinates (location) of instability.

(e) A measure of confidence (i.e. a measure of expected error) in the prediction is assigned; this measure is related to the distance of the proposed location of instability from the centre of the reactor.

Prediction of the location of instability is successful when

(i) patterns of the simplified model are used for training, validating and testing the ANNs,
(ii) patterns from the "actual physical system" are used for training, validating and testing the ANNs.

When patterns of the simplified model are used for training and validation of the ANNs and patterns from the "actual physical system" are used for testing, instability localization is:

(I) accurate in the central part of the reactor,
(II) approximate near the boundaries of the reactor; in this case, the prediction is shrunk towards the centre by an amount related to the distance of the predicted location from the centre of the reactor, while it is extended towards the boundaries of the reactor for locations of instability in the vicinity of either detector.

The less-than-perfect performance observed is not a matter of ANN construction/training or of ANN response combination, but a matter of characteristic differences (discrepancy in the neutronic responses and, subsequently, the response-ratios) between the two models:

- The simplified model ignores the "peaking effect" of the "actual physical system"; consequently, the latter deviates significantly from the simplified model at locations of instability in the vicinity of the detectors.
- Larger response-ratios occur for locations of instability near the boundaries of the reactor. As a result, shrinkage of the predicted location of instability towards the centre of the reactor is observed when performing instability localization using patterns from the "actual physical system" corresponding to locations of instability near the boundaries of the reactor.

An improved model of the "actual physical system", and — in practice — an adequately good model of the reactor, should be expected to be able to reasonably localize the instability employing the proposed approach.

References

Behringer, K., Kosaly, G., Kostic, Lj., 1977. Theoretical investigation of the local and global components of the neutron-noise field in a boiling water reactor. Nuclear Science and Engineering 63, 306–318.

D' Auria, F. et al., 1997. State of the art report on boiling water reactor stability. NEA/CSNI/R(96) 21, 247.

Engstrom, S., 1996. Forsmark internal report FT-Rapport 96/326 (in Swedish).

Haykin, S., 1994. Neural Networks — A Comprehensive Foundation. Prentice-Hall, USA.

Karlsson, J.K.-H., Pazsit, I., 1999. Localization of a channel instability in the Forsmark — 1 boiling water reactor. Annals of Nuclear Energy 26, 1183–1204.

Pazsit, I., Glocker, O., 1983. On the neutron noise diagnostics of pressurized water reactor control rod vibrations — I: periodic vibrations. Nuclear Science and Engineering 85, 167–177.

Pazsit, I., Glocker, O., 1984. On the neutron noise diagnostics of pressurized water reactor control rod vibrations — II: stochastic vibrations. Nuclear Science and Engineering 88, 77–87.

Pazsit, I., Glocker, O., 1988. On the neutron noise diagnostics of pressurized water reactor control rod vibrations — III: application at a power plant. Nuclear Science and Engineering 99, 313–328.

Pazsit, I., Garis, N.S., Glocker, O., 1996. On the neutron noise diagnostics of pressurized water reactor control rod vibrations — IV: application of neural networks. Nuclear Science and Engineering 124, 167–177.

Rumelhart, D.E., Hinton, G.E., Williams, R.J., 1986. Learning representations by back-propagating errors. Nature 323, 533–536.